Use of cubic structure with primitive nanochannels for fabrication of free standing 3D nanowire network of Pt with *Pm3m* symmetry

Samina Akbar [1,3], Joanne M. Elliott [1], Adam M. Squires [1,2], and Aneela Anwar [3]*

[1] Department of Chemistry, University of Reading, Whiteknights, Reading, RG6 6AD, UK

[2] Department of Chemistry, University of Bath, Bath BA2 7AY, UK

[3] Department of Basic Sciences and Humanities, University of Engineering and Technology New Campus, Lahore, Pakistan

***Corresponding Author**

Samina Akbar

s.akbar@uet.edu.pk

Department of Basic Sciences and Humanities, University of Engineering and Technology New Campus, Lahore, Pakistan

Keywords: Template, liquid crystals, primitive cubic, platinum, nanoporous

Abstract

In this work, we developed a lipid mixture based on phytantriol / polyoxyethylene surfactant (Brij-56) that forms a *Im3m* symmetry bicontinuous cubic phase based on the Schwartz primitive surface (Q_{II}^{P}), from which we templated highly ordered 3D nanoporous platinum with a novel "single primitive" morphology (*Pm3m* symmetry). The Q_{II}^{P} template phase is obtained by incorporation of 17.5 % w/w Brij-56 ($C_{16}EO_{10}$) (a type-I surfactant) into phytantriol under excess hydration conditions. Phytantriol alone forms the double diamond Q_{II}^{D} (*Pn3m*) phase, and in previous studies incorporating Brij-56 at different compositions

the cubic phase maintained this morphology, but increased its lattice parameter; mesoporous metals templated from these Q_{II}^{D} lipid templates all exhibited the "single diamond" (*Fd3m*) morphology. In contrast, the current paper presents the availability of our Q_{II}^{P} cubic phases to template nanoporous materials of single primitive *Pm3m* morphology via chemical and electrochemical methods. To explore the structure porosity and morphological features of the templated Pt material, X-Ray Scattering and Transmission Electron Microscopy (TEM) are used. The resulting 3D nanoporous Pt materials are found to exhibit a regular network of Pt nanowires of ~ 4 nm in diameter with a unit cell dimension of 14.8 ± 0.8 nm, reflecting the aqueous network within the Q_{II}^{P} template.

Introduction

A remarkable breakthrough to advance nanomaterials identifies innovative scientific achievements in the field of catalysis,[1,2] photonics,[3] optoelectronics,[4] and adsorption.[5] Due to their most intriguing structural features, 3D nanoporous materials of metal and semiconductors exhibit unique optical,[6] electronic,[7] magnetic,[8] and catalytic[9] properties desirable for various applications in modern efficient electronic devices including batteries,[10] fuel cell,[11] solar cells,[12] chemical and biochemical sensors.[13] Efforts are being made to design mild, inexpensive, and environment friendly routes to synthesise materials with nano-confinements ranging from 1–100 nm in size.[14-16] Specifically, these nanoporous materials including metals and non-metals can be synthesized by templating assisted by chemical or electrochemical methods.[17] Besides the excellent control over the nanoarchitecture, the templating approach also enables precise tuning of structural parameters in nanoporous materials. For this, most of the studies reported the use of exotemplate (hard templates) such as porous Alumina[18], and porous carbon[19]. But their multi step lengthy procedures under harsh conditions are the main limitation to these approaches. As compare to these traditional templating methods,[20,21] soft templating method using diblock co-polymers[22] and surfactant

based liquid crsytal systems,[23] is much more adoptable and can effectively control the morphology, pore size, pore orientation, and pore to pore distance in nanomaterials.[24,25] Soft templating using amphiphilic surfactant for the synthesis of nanoporous structures has been reported in various studies[24,26,27] since its first use by Attard *et al.*,[23] where 2D mesoporous materials were simply replicated using surfactant based hexagonal template. 3-dimentionality in nanoporous materials is of great technological importance, as it overcomes the problem of interconnectivity associated with 1D and 2D structures, and offer great accessibility with enhanced diffusion of dissolved species[28,29] and fast electron transport properties.[7] Nanoporous materials exhibiting 3D networks of nanowire with highly sophisticated architectural properties are an emerging class of materials. Well-ordered interconnected nanowire networks of Pt[9] and TiO_2[30] have been replicated using degradable block co-polymers as a template. But lengthy procedures and harsh conditions used in these studies, promoted the scientist to find an alternative template for the synthesis of 3D nanoporous materials.

Lipidic inverse bicontinuous cubic phases (Q_{II}) owing to their most fascinating structural features are highly desirable for promising applications in biomedical science[31,32]. New advances in the potential applications of cubic phases towards the synthesis of 3D nanoporous materials have been emerged in the recent years.[33-35] As compared to other liquid crystal phases, high viscosity of cubic phases has been the major hindrance toward their applications in templating. However, substrate modification using thin layer coating approach was a major breakthrough in cubic phase templating.[35] The use of type II (inverse) bicontinuous cubic phases for templating of nanomaterials has been accelerated since their first use in 2013.[33,35-37]

Bicontinuous cubic structures are comprised of highly curved lipid bilayer extending into three dimension fashion surrounded by water on both sides, forming two continuous but non-

intersecting aqueous channels.[38,39] Depending upon crystallographic space group symmetry, inverse bicontinuous cubic phases can be identified as double diamond (Q_{II}^{D}, *Pn3m*), double gyroid (Q_{II}^{G}, *Ia3d*), and double primitive (Q_{II}^{P}, *Im3m*).[40] These three phases represent double network structures. In gyroid and diamond phases, the two water channel networks meet at 120^{o} in three way junction and at 109.5^{o} in four way junction respectively. However, in primitive phase, the two networks meet at 90^{o} in six way junction.[41] Simulations of such kind of 3D networks with 6-fold 90° junctions (as in the primitive structure) show a significant effect of nanostructure on reducing thermal conductivity in semiconductor materials through phonon scattering, especially if the lattice parameter approaches the wavelength of thermal phonons, below 10 nm.[42] Although the present paper demonstrates formation of a primitive structured Pt metal, where thermal conductivity by free electrons would dominate, the paper represents proof of concept that the Q_{II}^{P} phase templates can successfully be used to produce nanoporous metals/semiconductors replicating water channel symmetry[36] and holds tremendous potential toward nanomaterials engineering.

Further, unlike the diamond and gyroid structures, the primitive structure contains straight channels and wires. These have implications for transport and diffusion, and also for containment of long, linear particles. For example, the lipid Q_{II}^{P} phase has been shown to be better able to accommodate siRNA.[43] Further, there is great deal of interest lies in structural designing of these nanostructures. It has been reported that primitive structure are more responsive to lattice swelling as compare to diamond structure.[44] Thus, these templates could help facilitate the architectural tuning of replica materials and hold tremendous potential toward nanomaterials engineering.

Phytantriol is a chemically sable and inexpensive amphiphile molecule capable of self-assembly in aqueous environment. Structure and morphology of self-assembled liquid crystalline phases depends upon temperature and the concentration of phytantriol.[45] Under

excess hydration conditions, phytantriol exhibits stable bicontinuous cubic phase of diamond morphology which has been successfully used as a template for the fabrication of mesoporous metals with single diamond morphology (Fd3m symmetry).[34,35] It has been reported that phytantriol phase behaviour is very sensitive to the presence of any impurity.[46] After incorporating Brij-56 at different compositions under excess hydration condition, the cubic phase (Q_{II}^{D}) maintained its morphology as reported in our previous study.[47] However, a noticeable increase in lattice parameter was observed at specific Brij-56 compositions (7.5 and 20% w/w Brij-56 in phytantriol). It was proposed that addition of Brij-56 reduced the curvature of lipid bilayer which resulted in swelling of diamond cubic phase structure. Mesoporous Pt metal templated from these swelled Q_{II}^{D} lipid templates all exhibited the "single diamond" (*Fd3m*) morphology with increased unit cell size.[47]

Among the three bicontinuous cubic phases, the primitive phase is the least curved phase and does not appear in pure phytantriol/water systems. However, it is reported that in the presence of additives, Q_{II}^{D} phase adopts the Q_{II}^{P} phase morphology.[48,49] The current work shows such an adaptation of cubic phases in phytantriol where Q_{II}^{D} phase acquired Q_{II}^{P} morphology in the presence of specific composition of Brij-56 under excess hydration conditions. Further, in this study, Q_{II}^{P} phase for the very first time is exploited as a template for the fabrication of nanoporous Pt materials Electrochemical and chemical assisted templating successfully produced previously unreported highly stable free standing 3D Pt nanowire networks of single primitive morphology with *Pm3m* symmetry.

Experimental

Chemicals and Materials: Phyantriol ($C_{20}H_{42}O_3$) (purity >98.3 %), was donated by Adina Cosmetics Ingredients UK. Hexachloroplatinic acid (H_2PtCl_6) (8 wt% solution in water) and Brij-56 ($C_{16}EO_{10}$) were used as received from Aldrich. p.a.-grade Conc. H_2SO_4 was

purchased from Merck. Ethanol (laboratory reagent grade) was purchased from Fischer Scientific. Deionized, double distilled water was further purified by passing through a water purification system (Milli Q) and used for the preparation of solutions. A 2 mm thick stainless steel sheet (Inspired steel limited), was cut down to 1 cm^2 small pieces at in-house mechanical workshop.

Preparation of templating mixture (primitive cubic liquid crystal phase): To prepare binary mixtures of phytantriol containing17.5 % Brij-56 (w/w) of total weight (phytantriol + Brij-56), appropriate amount of Brij-56 and phytantriol was weighed in a glass vial followed by vigorous mixing with the help of a spatula (polypropylene) at room temperature. The vials were sealed and heated at 40^oC for max. 20 min in water bath and then cooled down to room temperature. After mixing, air bubbles were removed by letting the samples to rest for max. 2 hours.

Ethanolic solutions of templating mixtures: Depending upon the requirements, phytantriol or the binary mixtures of phytantriol/Brij-56 were each dissolved in ethanol in 1:1 (for SAXS analysis) or in 1:2 ratios (w/w) (for deposition) in capped glass vials followed by sonication for 20-30 mins.

Preparation of Liquid crystal samples for SAXS analysis: Ethanolic solution of templating mixture was coated inside a thin-walled glass capillary tube using method reported in SI (1.1). The inside coated glass tubes were filled with HCPA solution or water, sealed, and rested for min. 10 minutes prior to analysis.

Chemical deposition: A steel plate fixed in a Teflon cell with a hole of 3.14 cm^2 area was coated with a thick layer of phytantriol (1-2 mm) using their ethanolic solution of phytantriol containing 17.5% Brij-56. Ethanol was allowed to evaporate for 1-2 hour under ambient conditions followed by dropwise addition of HCPA solution (~2 – 3 ml). The cell was left for max. 8 hours until the mixture turns black. The mixture containing Pt deposits was removed

from the Teflon cell and collected in a glass vial followed by washing using procedure reported in SI (1.2).

Electrochemical Experiments: For electrochemical experiments, a purposely built potentiostat [specifications are provided in SI (1.3)] was used. A simple three electrode system was used for electrochemical measurements, shown in Figure S1. A Pt flag as counter electrode, Ag/AgCl as reference electrode, and pre-polished Pt wire electrodes (of cross-sectional area 0.20 mm^2 sealed directly into glass) /Pt foil of area 1-5 mm^2 were used as working electrode.

Polishing of Pt wire electrodes was accomplished using procedure reported in SI (1.4).

Washing of electrodeposited Pt powder: After deposition, working electrodes were washed using ethanol and water. The procedure is described in SI (1.5).

SXAS analysis: Small Angle X Ray System shown in Figure S2 was used for recording of scattering patterns. Specifications of instrument and calibration details are given in SI (1.6). For analysis, Pt foil with electrodeposited nanoporous Pt material was directly attached to a sample grid with the help of polyimide sticky tape. In case of chemically deposited samples, a small amount of deposited Pt material was wrapped in a polyimide sticky tape and then was attached to the sample grid.

TEM analysis: Philips CM20 Transmission Electron Microscope (operation voltage: 200 kV) was used for imaging. A small amount of electrochemically deposited Pt was scrapped off from the substrate with the help of a scalpel and placed on a carbon film supported copper grid. Chemically deposited Pt was dissolved in 5 ml of acetone and sonicated for at least 5 min. A drop of the solution was then placed on the TEM grid for analysis.

Results and discussion

Phase behaviour of phytantriol in the presence of different w/w compositions of Brij-56 in phytantriol was studied under excess hydration conditions. Phase behaviour diagram of

phytantriol in the presence of Brij-56 under excess hydration conditions is shown in Figure S3. Cubic phase of primitive morphology (Q_{II}^{P}) was observed over a small region exists between 10 to 20 % Brij-56 (w/w) in phytantriol. At 17.5 %(w/w) Brij-56 composition, Q_{II}^{P} phase was stable up to 35 ^{o}C. 1-D SAXS profiles for Phytantriol containing 0% and 17.5% (w/w) Brij-56 in excess water at 20 ^{o}C are shown in Figure 1. SAXS pattern (figure 1,A) for phytantriol in excess water without the presence of Brij-56 shows six Bragg peaks with the relative positions for 1/d in the ratio √2, √3, √4, √6, √8, √9 which can be indexed as 110, 111, 200, 211, 220, 221, consistent with the cubic phase Q_{II}^{D} of space group *Pn3m*. Lattice parameter was estimated to be 6.8 ± 0.2 nm. For phytantriol containing 17.5% Brij-56 (w/w) in excess water, Bragg peaks representing Q_{II}^{D} phase disappeared completely giving rise to three new peaks of almost equal intensity corresponding to the presence of cubic phase Q_{II}^{P} of primitive morphology with space group *Im3m*.[50] Lattice parameter was estimated to be 14.7 ± 0.1 nm. It is assumed that Brij-56, a type I surfactant, is penetrated to the phytantriol bilayer at the polar/apolar interface region which leads to a reduction of monolayer curvature and flattening of the lipid bilayer.[51] Hence, curvature is modulated and as a result less curved phase (Q_{II}^{P}) [52,53] appear after incorporation of 17.5% Brij-56 into phytantriol bilayer as supported by SAXS patterns show in Figure 1,B.

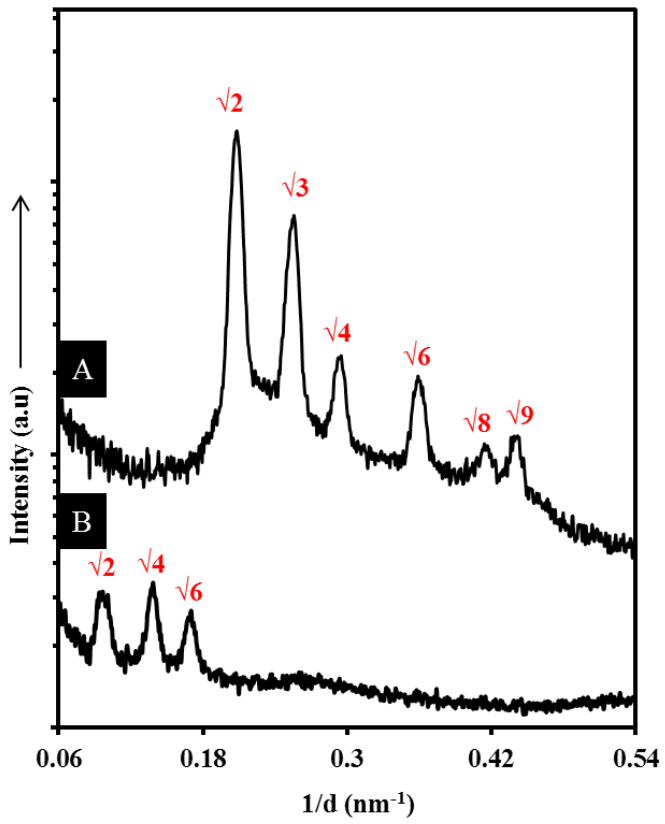

Figure 1: 1-D SAXS profiles for Phytantriol containing 0% (A) and 17.5% (B) (w/w) Brij-56 of total phytantriol + Brij-56 in excess water at 20 ^{o}C. Lattice parameter values of 6.8 ± 0.2 and 14.7 ± 0.1 nm are estimated for (A) and (B) respectively.

1-D SAXS profiles for phytantriol containing 17.5 %(w/w) Brij-56 in excess HCPA solution is shown in Figure 2(a). Three Bragg peaks are observed with the relative positions for 1/d in the ratio √2, √4, √6 consistent with the primitive cubic phase (Q_{II}^{P}).[50] For Q_{II}^{P} phase in excess HCPA, the lattice parameter is estimated to be 14.8 ± 0.1 nm. Thus no significant change in the lattice parameter was observed in the presence of platinum species within the aqueous nanochannels of the Q_{II}^{P} phase. Deposition of platinum within the nanochannels of the Q_{II}^{P} phase was carried out electrochemically. A typical electrodeposition transient is shown in Figure S4. 1-D SAXS profile of deposited nanostructured Pt film shown in Figure 2(b) shows a prominent Bragg peak with a *d*-spacing value of 10.5 ± 0.4 nm. A very small hump appears on left side of the peak with the *d*-spacing value of 14.7 nm. The values are not agreeing with the primitive cubic of symmetry *Im3m*. Interestingle, the two peaks with their relative positions for 1/d in the ratio √1 : √2, may correspond to first two reflection of single prmitive cubic of symmetry *Pm3m*. These can be indexed as *hkl* = (100), and (110). Considering *d*-spacing value of prominent Bragg peak, lattice parameter was estimated to be 14.8 ± 0.8 nm.

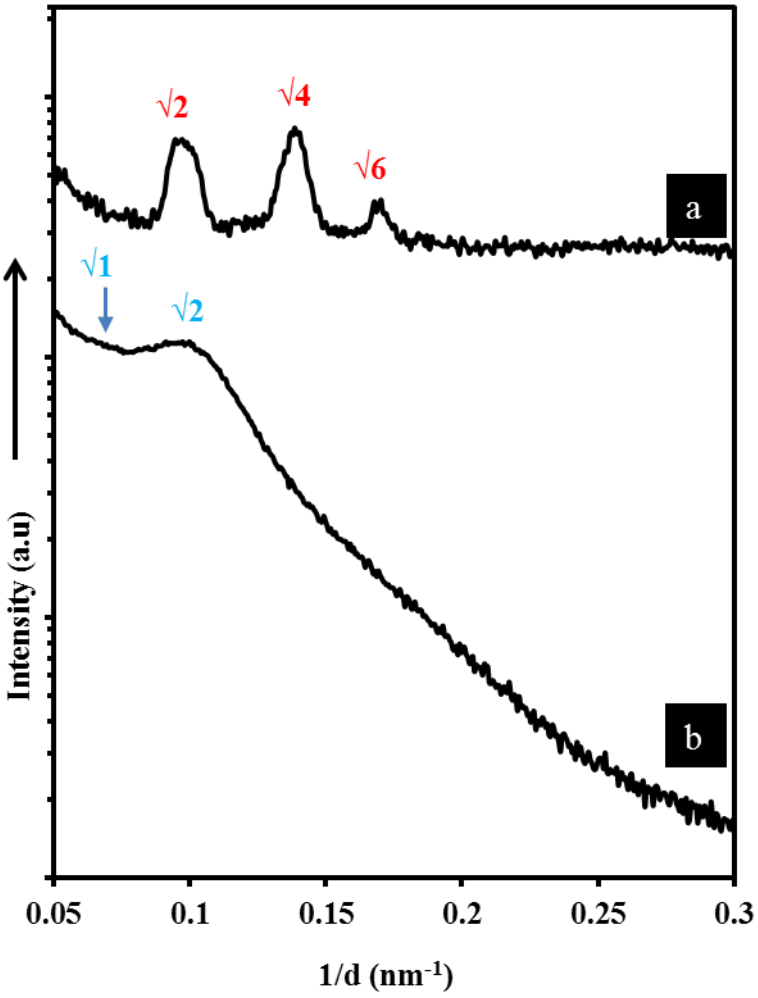

Figure 2: 1-D SAXS profiles for a) Phytantriol containing 17.5% (w/w) Brij-56 in excess HCPA solution and b) electrochemically fabricated nanoporous Pt, deposition charge density (Q) = 3.6 C cm^{-2}.

More informaion about the structural morphology is deduced from TEM analysis. The value of lattice constant obtained from TEM micrographs is compared with SAXS-estimated values. For TEM analysis, nanoporous Pt material is deposited chemically using steel as a source of electrons. SAXS profile of chemically deposited nanostructured Pt powder is shown in Figure S5. TEM micrographs taken at different resolution revealed that the deposited nanoporous Pt material is composed of 3D regular networks of Pt nanowires of ~ 4 nm in diameter. In Figure 3(a), a typical TEM micrograph of the chemically deposited nanoporous material shows a 3D nanowire network of Pt. The network runs parallel through several interconnected nanoparticles indicating their origin from single liquid crystal domain.[54] Figure 3(b) shows high magnification TEM micrograph highlighted from boxed area as shown in Figure 3(a). The particle exhibits edges and corners representing a crystal

like morphology. Many projections are simulated in various viewing directions. A model single primitive structure (c) viewing through (111) direction gives the best possible match which shows a triangular lattice, where each side of the triangle was estimated to be $a_p.\sqrt{2}$ = 18.9 ± 1.2 nm. Figure 2(d) shows another low resolution TEM micrograph. Viewing through the single primitive structure (f) along (211) direction shows a long stripe pattern, similar to that observed in high magnification TEM micrograph shown in Figure 3(e) which was taken from boxed area shown in Figure 3(d).

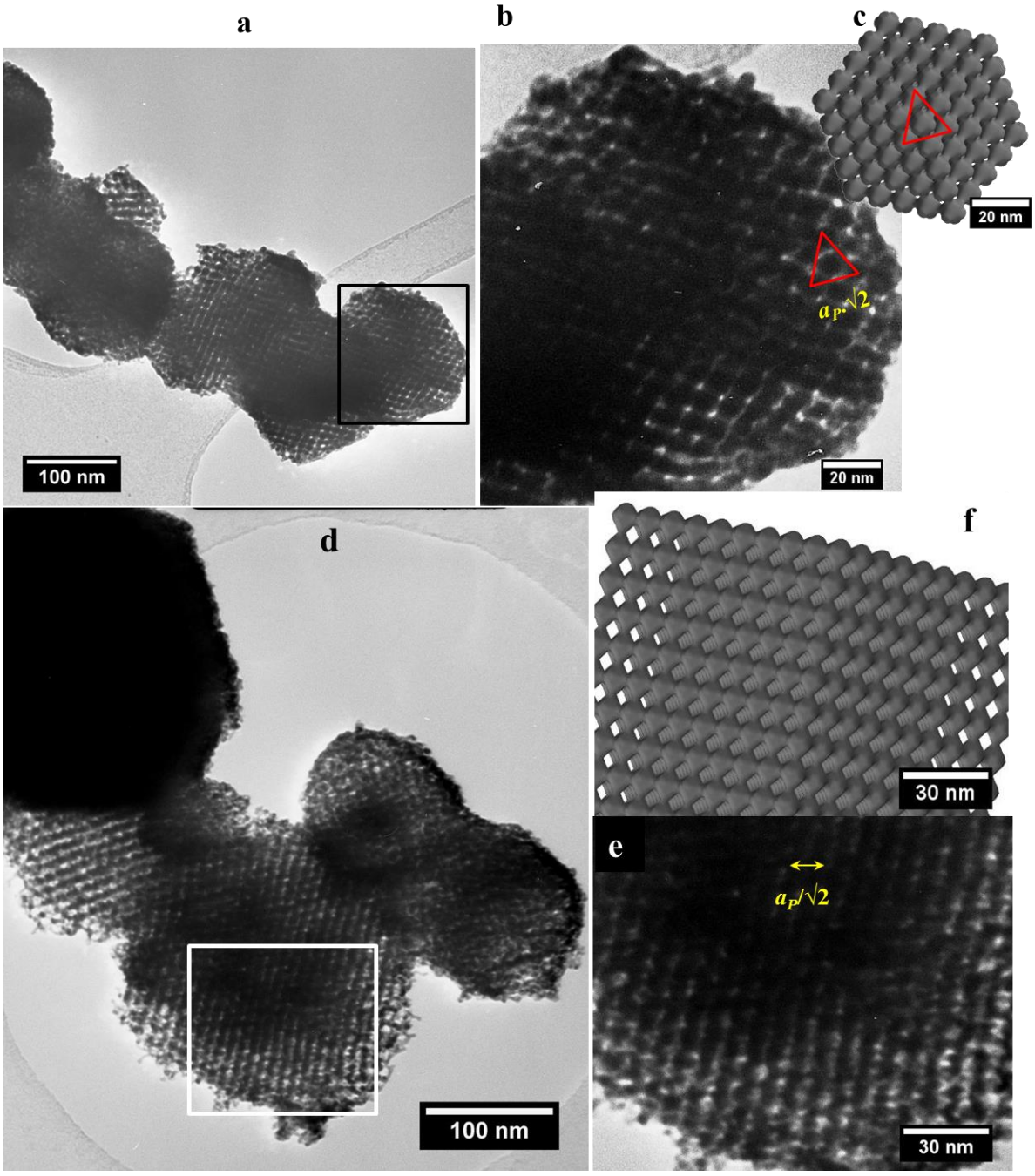

Figure 3: a) Low magnification TEM micrograph for chemically deposited nanostructured Pt, b) High magnification TEM micrograph from the boxed area shown in "a", c) a simulated projection from *Pm3m* symmetry along (111) direction, d) LR TEM micrograph of chemically deposited nanostructured Pt, e) HR TEM micrograph from the boxed area shown in "d" and a simulated projection (f) of *Pm3m* symmetry along 211 direction.

From Figure 3(e), the centre to centre distance between the two adjacent stripes was estimated to be $a_p/\sqrt{2}$ = 10.4 ± 0.9 nm. TEM-estimated lattice parameter values well agrees with SAXS estimated lattice parameters valuse assuming a single primitive bicontinuous of symmetry (*Pm3m*). On the basis of SAXS data and TEM analysis,we suggested that the structure of the deposited nanoporous Pt material is arrised by asymmetric templating[55], supporting the presence of single primitive structure of symmetry *Pm3m*.

However, the SAXS data cannot explain the absence of many other reflections ($\sqrt{3}$, $\sqrt{4}$, etc) that may arise from the single primitive cubic phase of symmetry *Pm3m*. Although the *Pm3m* symmetry suggests positions for peaks, but it does not predict the intensity, which depends upon the electron density distribution within the unit cell. As we are not modeling this, it is possible that this structure happens to give very weak reflections.

A cartoon structure of the double primitive cubic Q_{II}^{P} phase of *Im3m* symmetry which consists of two water channel networks, the corresponding bilayer, and the resulting single primitive cubic structure of *Pm3m* symmetry is shown in Figure 4.

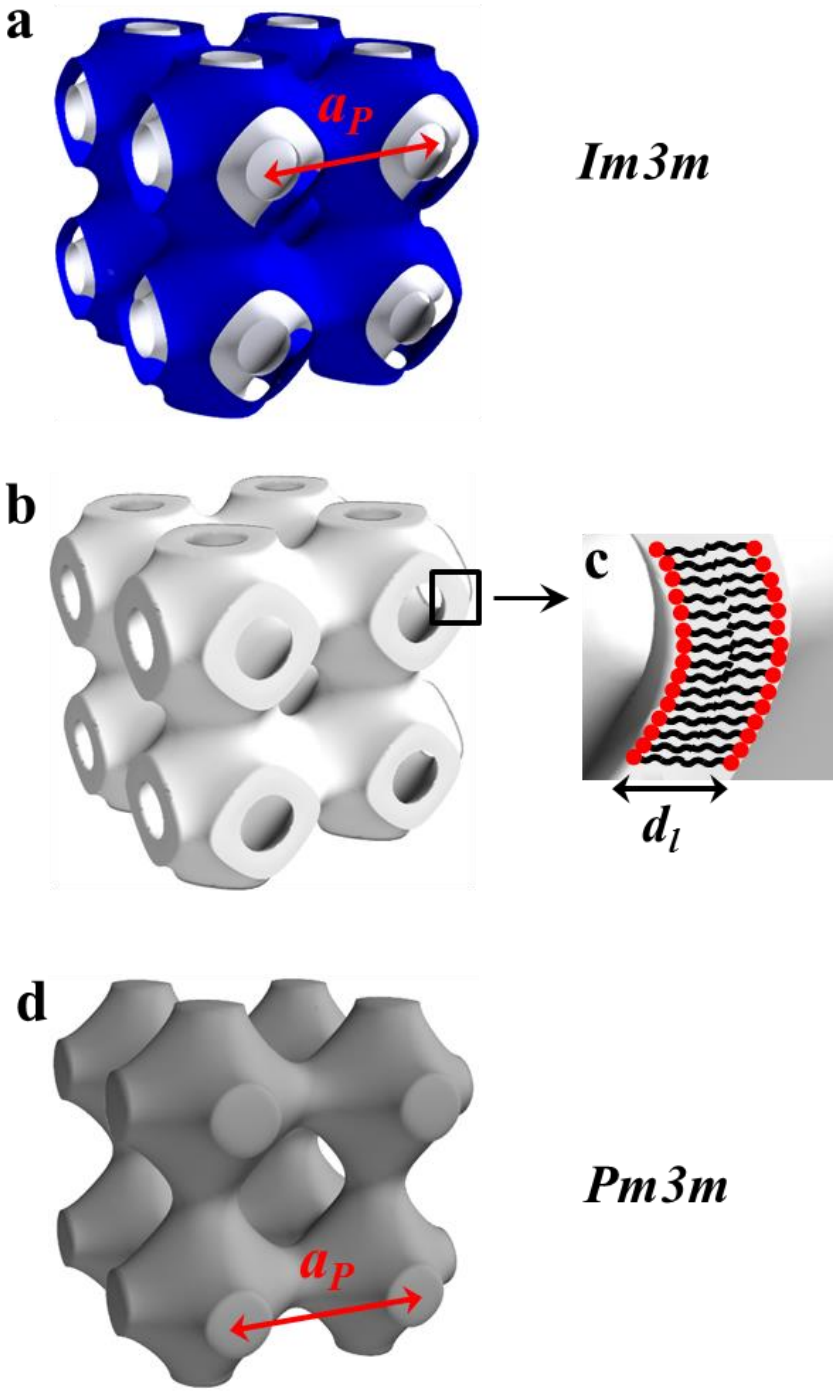

Figure 4: Structure of a) the two water channel network in a double primitive bicontinuous cubic (Q_{II}^P) phase of symmetry *Im3m*, b) the corresponding lipid bilayer, c) a bilayer arrangement of surfactant molecules, and d) the resulting templated single primitive structure of symmetry *Pm3m*. a_P and d_l represent the lattice parameter and the bilayer thickness respectively.

The unit cell dimensions (a_P) remains constant in double primitive (*Im3m*) and its lower symmetry counterpart single primitive (*Pm3m*). Therefore the lattice parameter values observed for the Q_{II}^P phase used as a template and the templated nanoporous Pt material agree well.

For electrochemical investigation, nanostructured Pt films were fabricated on Pt wire electrodes coated with thin film of phytantriol containing 17.5 %(w/w) Brij-56. After deposition and washing, to determine the electrochemical accessibility of nanoporous Pt, electrodes are cycled in dilute aqueous H_2SO_4 between the limit +1.2 to -0.25 V vs Ag/AgCl. The voltammogram recorded for 3D nanoporous Pt show well defined regions for hydride adsorption/desorption and oxygen adsorption/desorption which show the absence of any organic impurities from the surfactant used as a template (phytantriol or Brij-56). Voltammetric peaks in the H_{upd} region suggest the polycrystalline nature of the nanostructured platinum[56]. For the catalytic applications, it is highly desirable that the electroactive surface area per unit geometric area of the electrode should be controllable. In order to investigate the potential of nanoporous Pt films towards such applications, deposition was carried out through the phytantriol based Q_{II}^P phase in the presence of 17.5 %(w/w) Brij-56 at a deposition charge density ranging from 1 to 6 C cm^{-2} at platinum electrodes (1.9635E-03 cm^2) at room temperature. The corresponding Rf values are determined and a graph was plotted for Rf values vs deposition charge density values, as shown in Figure 5(b). Linear relationship demonstrates the uniform accessibility of free standing 3D nanoporous Pt material. Deposited free standing 3D nanoporous Pt film increased the original 1.9635E-03 cm^2 Pt electrode area by a factor of 134 for one coulumb charge density. Presumably charge density (Q) is directly proportional to the deposited platinum mass, and therefore to the effective surface areas. Thus controlling the charge density for deposition of Q_{II}^P-ePt films, electroactive surface area per geometric area of the electrode can be controlled at will.

The electrochemical stability of the nanostuctured Pt films was investigated by repeated cycling in dilute H_2SO_4 (0.5 M) between the limits -0.35 to +1.2 V vs Ag/ACl at 0.2 V s^{-1} scan rate. Cyclic voltammograms before and after cycling are compared in Figure S6. No observable change in the peak currents was found in the cyclic voltammograms which confers the high electrochemical and mechanical stability of the nanoporous Pt films, desirable for their potential applications in electrocatalysis[57,58].

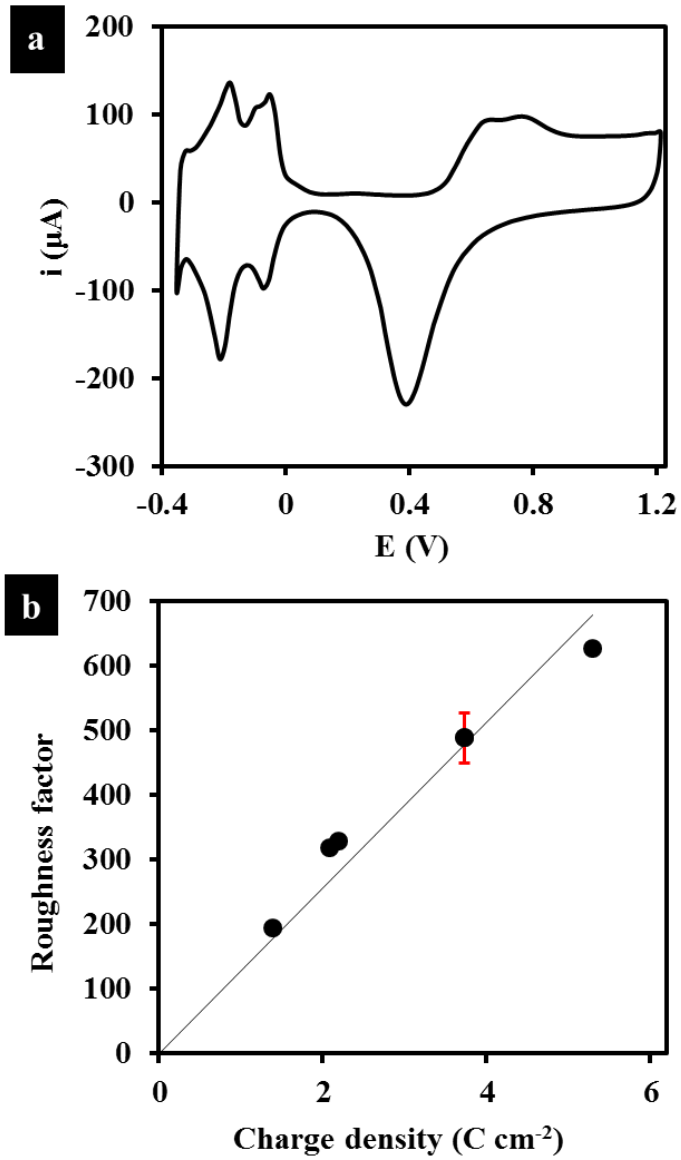

Figure 5: a) Cyclic voltammograms of a nanostructured Pt electrode recorded in 0.5 M aqueous H_2SO_4 at 0.2 V s^{-1} scan rate vs Ag/AgCl, deposited at -0.2 Vat room temperature with a deposition charge density of 2.19 C cm^{-2}, Rf value was estimated to be 329. b) Plot of Rf values vs charge density for nanostructured Pt material electrodeposited through the Q_{II}^{P} phase of phytantriol containing 17.5 %(w/w) Brij-56 in excess HCPA. In all cases, electrodeposition was carried out at -0.2 V vs Ag/AgCl at room temperature at platinum electrodes with the area 1.96 x 10^{-3} cm^2.

Summary

A novel, highly ordered free standing 3D network of Pt nanowires is fabricated through direct liquid crystal templating. In this study, primitive cubic (Q_{II}^{P}) phase of symmetry *Im3m*, is

employed for templating of nanoporous Pt materials. The Q_{II}^{P} phase appears in the phytantriol/water system upon the incorporation of 17.5 %(w/w) Brij-56. The unique 3-D channel network of primitive cubic phase acted as a nanoporous host for the Pt species. Reduction of Pt species within one of the aqueous channels led to the formation of highly ordered 3D network of platinum nanowires of single primitive morphology of *Pm3m* symmetry. The nanoporous Pt material was successfully fabricated using both chemical and electrochemical methods. SAXS data and the TEM investigations supported the presence of highly porous structure of symmetry *Pm3m*. Electrochemical investigations showed that the free standing 3D Pt nanowire network exhibit very high surface area, excellent accessibility, and electrochemical stability, revealing their potential toward catalytic applications. This study explores the availability of primitive cubic phases, for the first time, as a template to produce Pt nanomaterials of relatively new morphology that could accelerate progress toward the synthesis of 3D semiconductor materials to achieve the scientific goals at next generation level.

References

1. Liu, M., *et al.*, *Advanced Materials* (2019) **31** (6), 1802234
2. Xia, W., *et al.*, *Angewandte Chemie International Edition* (2016) **55** (8), 2650
3. Mishra, Y. K., *et al.*, *Vacuum* (2017) **146**, 304
4. Suzuki, T., *et al.*, *The Journal of Physical Chemistry C* (2008) **112** (6), 1831
5. Clavilier, J., *et al.*, *Journal of electroanalytical chemistry and interfacial electrochemistry* (1986) **205** (1-2), 267
6. Dehmel, R., *et al.*, *Macromolecules* (2017) **50** (16), 6255
7. Sheng, X., *et al.*, *Nano letters* (2014) **14** (4), 1848
8. Alam, S., *et al.*, *Angewandte Chemie* (2009) **121** (40), 7494
9. Cheng, C.-F., *et al.*, *NPG Asia Materials* (2015) **7** (4), e170
10. Lu, Y., *et al.*, *Journal of Solid State Electrochemistry* (2012) **16** (5), 1863
11. Guo, S., and Wang, E., *Nano Today* (2011) **6** (3), 240
12. Lan, Z., *et al.*, *Journal of Materials Chemistry* (2012) **22** (9), 3948
13. Tee, S. Y., *et al.*, *Materials Science and Engineering: C* (2017) **70**, 1018
14. Akbar, S., *et al.*, *Materials Science and Technology* (2019) **35** (1), 1
15. Li, L.-L., *et al.*, *Journal of Materials Chemistry* (2012) **22** (13), 6267
16. Xie, Y., *et al.*, *Journal of Nanomaterials* (2016) **2016**, 2302595
17. Meseck, G. R., *et al.*, *Current Opinion in Colloid & Interface Science* (2017) **29**, 9
18. Wang, D., *et al.*, *small* (2013) **9** (7), 1025
19. Lee, J., *et al.*, *Advanced materials* (2006) **18** (16), 2073
20. Fukuoka, A., *et al.*, *Nano Letters* (2002) **2** (7), 793
21. Wang, H., *et al.*, *Journal of the American Chemical Society* (2011) **133** (37), 14526
22. Hamley, I., *Nanotechnology* (2003) **14** (10), R39
23. Attard, G. S., *et al.*, *Science* (1997) **278** (5339), 838
24. Akbar, S., *et al.*, *Langmuir* (2018) **34** (24), 6991
25. Asghar, K. A., *et al.*, *ACS nano* (2015) **9** (11), 10970

26. Seddon, J. M., and Raimondi, M. E., *Molecular Crystals and Liquid Crystals Science and Technology. Section A. Molecular Crystals and Liquid Crystals* (2000) **347** (1), 221
27. Chawla, M., *et al.*, *Journal of Molecular Catalysis A: Chemical* (2016) **423**, 126
28. Kaasgaard, T., and Drummond, C. J., *Physical Chemistry Chemical Physics* (2006) **8** (43), 4957
29. Ghanbari, R., *et al.*, *The Journal of Chemical Physics* (2019) **150** (9), 094901
30. Crossland, E. J. W., *et al.*, *Nano Letters* (2009) **9** (8), 2807
31. Zabara, A., *et al.*, *Small* (2013) **9** (21), 3602
32. Nazaruk, E., *et al.*, *Analytical and bioanalytical chemistry* (2008) **391** (5), 1569
33. Akbar, S., *et al.*, *Journal of Nanoparticle Research* (2020) **22** (6), 1
34. Burton, M. R., *et al.*, *Scientific Reports* (2017) **7** (6405),
35. Akbar, S., *et al.*, *Advanced Materials* (2013) **25** (8), 1160
36. Burton, M., *et al.*, *Scientific Reports* (2017) **7** (1), 1
37. Richardson, S., *et al.*, *Nanoscale* (2016) **8** (5), 2850
38. Tiddy, G. J. T., *Physics Reports* (1980) **57** (1), 1
39. Wagner, E., *Parfuem. Kosmet.* (1994) **75**, 260
40. Scriven, L., *Nature* (1976) **263** (5573), 123
41. Squires, A. M., *et al.*, *Physical Review E* (2005) **72** (1), 011502
42. Verdier, M., *et al.*, *arXiv preprint arXiv:1802.05654* (2018),
43. Kim, H., and Leal, C., *ACS Nano* (2015) **9** (10), 10214
44. Leung, S. S. W., and Leal, C., *Soft matter* (2019) **15** (6), 1269
45. Barauskas, J., and Landh, T., *Langmuir* (2003) **19** (23), 9562
46. Dong, Y.-D., *et al.*, *Langmuir* (2008) **24** (13), 6998
47. Akbar, S., *et al.*, *ACS Applied Nano Materials* (2021) **4** (6), 5717
48. Barauskas, J., *et al.*, *Nano Letters* (2005) **5** (8), 1615
49. Tilley, A., *et al.*, *Physical Chemistry Chemical Physics* (2011) **13** (8),
50. Luzzati, V., *et al.*, Chapter 1 The Cubic Phases of Lipids. In *Current Topics in Membranes*, Richard, M. E., (ed.) Academic Press, (1997), Vol. Volume 44, pp 3
51. Angelova, A., *et al.*, *Accounts of Chemical Research* (2011) **44** (2), 147
52. Shearman, G. C., *et al.*, *Journal of Physics: Condensed Matter* (2006) **18** (28), S1105
53. Richard H, T., *Current Opinion in Colloid & Interface Science* (1998) **3** (3), 255
54. Yamauchi, Y., *et al.*, *Electrochimica Acta* (2007) **53** (2), 604
55. Seddon, J. M., *Biochemistry* (1990) **29** (34), 7997
56. Bard, A. J., and Faulkner, L. R., *Electrochemical methods : fundamentals and applications*. Wiley: New York, 1980,
57. Koenigsmann, C., and Wong, S. S., *Energy & Environmental Science* (2011) **4** (4), 1161
58. Rauber, M., *et al.*, *Nano Letters* (2011) **11** (6), 2304